Title
Defining the contributions of permanent electrostatics, Pauli repulsion, and dispersion in density functional theory calculations of intermolecular interaction energies

Journal
The Journal of Chemical Physics, 144(11)

ISSN
0021-9606

Authors
Horn, Paul R
Mao, Yuezhi
Head-Gordon, Martin

Publication Date
2016-03-21

DOI
10.1063/1.4942921

Peer reviewed

Defining the contributions of permanent electrostatics, Pauli repulsion, and dispersion in density functional theory calculations of intermolecular interaction energies

Paul R. Horn,[1, a)] Yuezhi Mao,[1] and Martin Head-Gordon[1, b)]

Kenneth S. Pitzer Center for Theoretical Chemistry, Department of Chemistry, University of California, Berkeley, CA 94720 and Chemical Sciences Division Lawrence Berkeley National Laboratory Berkeley, CA, 94720 Phone: 510-642-5957 Fax: 510-643-1255

In energy decomposition analysis (EDA) of Kohn-Sham density functional theory calculations, the so-called frozen (or pre-polarization) interaction energy contains contributions from permanent electrostatics, dispersion, and Pauli repulsion. The standard classical approach to separating them suffers from several well-known limitations. We introduce an alternative scheme that employs valid antisymmetric electronic wavefunctions throughout and is based on the identification of individual fragment contributions to the initial supersystem wavefunction as determined by an energetic optimality criterion. The density deformations identified with individual fragments upon formation of the initial supersystem wavefunction are analyzed along with the distance dependence of the new and classical terms for test cases that include the neon dimer, ammonia borane, water-Na^+, water-Cl^-, and the naphthalene dimer.

[a)]Electronic mail: prhorn@berkeley.edu

[b)]Electronic mail: mhg@cchem.berkeley.edu

I. INTRODUCTION

A long-standing problem in electronic structure theory is the decomposition of the interaction energy of a system of fragments into several other scalars corresponding to physical concepts, such as charge transfer, permanent electrostatics, induced electrostatics, dispersion, and Pauli repulsion. Unfortunately, these quantities have no unique definition in the interesting part of the supersystem potential, corresponding to strongly to moderately interacting fragments. By contrast, in the very weakly interacting, non-overlapping regime, these physical concepts either have well-known definitions[1,2], or they are zero.

Accordingly, many schemes exist for performing an energy decomposition analysis (EDA) of the interaction energy[3–6]. As reviewed in detail below, many existing definitions neglect antisymmetry in the electronic wavefunction when computing the expectation values that define terms such as the Pauli repulsion and permanent electrostatic contributions. The purpose of this work is to introduce new and improved definitions for the permanent electrostatic, Pauli repulsion, and dispersion contributions for density functional theory (DFT) calculations. This problem is ripe for re-examination because of the recent flowering of DFT methods that are capable of good accuracy for the treatment of intermolecular interactions that include dispersion effects[7–10]. Examples include use of damped C_6 potentials[11,12], nonlocal correlation (NLC) functionals[13,14], and functionals that are optimized to include such components.[15–17]

We now consider the physical content of the contributions of interest. Pauli repulsion typically refers to steric or volume-exclusion effects, the marked increase in energy when two non-bonded atoms are forced to occupy the same space. Atoms have effective volumes due to the "kinetic energy pressure"[18] exerted by electrons. The smaller the available volume, the higher the total kinetic energy of the electrons contained within. Each electron can also be seen as occupying a finite volume because same spin electrons cannot have the same position, due to fermion statistics (the Pauli principle). Thus, when atoms are brought into close contact, the average volume available to each electron decreases, increasing the kinetic energy of the system. Pauli repulsion is sometimes referred to as exchange repulsion which seems to us a misnomer since exchange accounts for a degree of same-spin electron

correlation, an effect that is hardly repulsive in nature. Regardless of one's perspective, the term should always be repulsive (i.e. positive semidefinite).

The permanent electrostatic contribution describes the mean-field coulomb interaction between the electrons and nuclei of each fragment with the electrons and nuclei of all others where the electronic structure of each species has not been allowed to relax in response to the presence of the other fragments. Differences in definitions arise from the important qualification about relaxation. All reduce to the easily understood classical electrostatic interaction between fragment charge distributions in the well-separated portion of the potential.

The permanent electrostatics term does not describe the interfragment electron-electron interaction in full, as it neglects their correlated motions. Separating correlation from mean-field behavior has proven to be both numerically and conceptually advantageous. Indeed, the asymptotic distance dependence of the interfragment electron correlation energy (the dispersion energy) is R^{-6}, which is usually distinct from permanent electrostatics. Dispersion, while relatively small in magnitude when the monomers involved are small, is manifestly attractive. It can thus be a key component of weak intermolecular interactions and a quite large component in interactions involving large monomers[2,10]. While dispersion has no unique definition in the overlapping regime, we can be sure that *not all* the correlation contributions to intermolecular interactions should be called dispersion, because the total can be net repulsive.[19] We will seek a "dispersion-like" term that is negative semi-definite and contains interfragment correlation contributions to binding that manifest R^{-6} behavior in the long range.

The majority of EDA methods employ a classical approach in which the permanent electrostatic term (E_{elec}^{cls}) is defined as the classical electrostatic interaction of the 3-space charge distributions (including nuclei) of fragments computed in isolation, $\{\rho_A^{tot}(\mathbf{r})\}$, and then translated to their respective positions in the complex.

$$E_{elec}^{cls} = \sum_{A<B} \int_{r_1} \int_{r_2} \rho_A^{tot}(\mathbf{r}_1) \frac{1}{\mathbf{r}_{12}} \rho_B^{tot}(\mathbf{r}_2) \tag{I.1}$$

$$\rho_A^{tot}(\mathbf{r}) = \rho_A(\mathbf{r}) + \rho_A^{nuc}(\mathbf{r}) \tag{I.2}$$

ρ_A is the total spinless 3-space density for the electrons of fragment A only.

The initial wavefunction is one in which electronic relaxation relative to the isolated fragment wavefunctions due to the presence of new species has not yet occurred. The anti-symmetric product of monomer wavefunctions is a common choice. As in Ref. 20, we term the interaction of unrelaxed complexes the frozen energy (E_{frz}):

$$E_{frz} = E_{init} - \sum_A E_A \tag{I.3}$$

The classical approach defines Pauli repulsion, E_{Pauli}^{cls}, as the non-electrostatic part of E_{frz}, decomposing the frozen energy as:

$$E_{frz} = E_{elec}^{cls} + E_{Pauli}^{cls} \tag{I.4}$$

Dispersion, on the other hand, is not treated in such a uniform way across EDA methods though it is sometimes taken as the DFT dispersion term itself especially in the case of Grimme's density independent corrections[11,12].

We now turn to the methods themselves. Bickelhaupt-Baerends EDA[4,21,22], KM EDA[23–25], and the CI-singles based scheme of Reinhardt et al.[26] all use the classical approach. Mandado and Hermida-Ramón[27], SRW-EDA[28], and ETS-NOCV[29–32] all similarly use the classical electrostatic term and the Heitler-London wavefunction with slight twists. Mandado and Hermida-Ramón[27] further decompose the Pauli term from the classical approach into an exchange term and a repulsion term. Likewise, SRW-EDA[28] and ETS-NOCV[29–32] can both optionally separate the classical Pauli term into a Pauli term and an electron-exchange or exchange-correlation term, respectively.

An important and widely used method for analyzing intermolecular interactions is Symmetry Adapted Perturbation Theory (SAPT)[1,33–39]. While it does use the classical approach for permanent electrostatics and Pauli repulsions, SAPT also defines a separate dispersion interaction. SAPT methods do not decompose the interaction energy from a DFT calculation. Instead the SAPT approach is itself a theory of intermolecular interactions.

Other EDA methods that use the classical approach include BLW-EDA[5,40–42] and PIEDA[43,44], but these methods also include separate dispersion terms. PIEDA assigns the entire correlation binding energy for each dimer as computed by a post-HF wavefunction method to dispersion. BLW-EDA exploits the structure of specific density functionals

that include a non-local correlation functional such as dDXDM[42,45,46]. The GKS-EDA[47–49] scheme likewise uses the classical electrostatic term; however, the Pauli term in this method is computed differently, using full exact exchange. It can also be further subdivided into exchange and repulsion. The GKS-EDA also computes a correlation term, from which a functional-specific dispersion contribution (e.g. Grimme's -D[11,12]) can be separated.

In the density-based EDA (DEDA)[50–52], the electrostatic interaction is computed classically; however, the initial wavefunction used to compute the Pauli repulsion term by difference is a Slater determinant minimized with the constraint that the density equals the sum of non-interacting fragment densities. This means that the total interacting complex density can be *exactly* expressed as the sum of undistorted fragment densities, and it stands in contrast to the antisymmetric product of monomer wave functions, for which the complex density is distorted relative to the simple sum. The classical electrostatic expression is therefore more appropriate in DEDA than in methods that use the frozen orbital model. We have recently studied the origin of the energy lowering in DEDA in detail[53] and showed that most is associated with interfragment electron delocalization, which is constant density charge transfer (CT). An additional constraint is necessary to avoid introducing this CT contribution to the frozen interaction[53], similar to the one used to prevent the contamination of polarization by CT[54].

Natural EDA (NEDA)[55–57], which is based on Natural Bond Orbitals (NBOs)[3,58], uses the classical approach to compute the electrostatic interaction but then defines its Pauli-repulsion-like term, core, rather differently in terms of polarized monomer Lewis structures. To this is usually added an exchange-correlation term, which is the exchange-correlation functional's contribution to the interaction of these polarized monomer Lewis structures. Natural Steric Analysis[59–61] is likewise based on NBO analysis and draws heavily from the orbital orthogonality interpretation of antisymmetry to define the steric energy. This scheme also allows for an approximate decomposition into pairwise local orbital contributions which can be intramolecular.

The method of de Silva and Korchowiec[62] uses the standard classical electrostatic term but computes the Pauli-repulsion-like term, called exchange, as the difference between the energy of a determinant describing the polarized supersystem and the energy of the sum of polarized

fragments' densities matrix. In DFTs-EDA[63,64], a separate steric term is computed as the Weizsäcker kinetic energy contribution to total binding, and a Pauli term is computed as the difference between this and the contribution to binding from the non-interacting Kohn-Sham kinetic energy. The remaining binding energy is divided into exchange-correlation functional contributions and electrostatics.

Other EDA methods do not attempt to further decompose the frozen (or steric) energy into permanent electrostatic, Pauli repulsion, or dispersion interactions. Examples include Reduced Variational Space (RVS)[25,65], Constrained Space Orbital Variations (CSOV)[66], and Absolutely Localized Molecular Orbital (ALMO)-EDA[20,67–69]. In the ALMO-EDA, the classical approach is avoided due to its reliance on a classical charge distribution that does not correspond to the charge distribution of the unrelaxed complex. However, the absence of distinct terms describing permanent electrostatics and Pauli repulsion is a limitation[6] because these concepts are important for understanding intermolecular interactions. It is thus the goal of this work to construct a more satisfying decomposition of the frozen energy for use in EDA schemes such as the ALMO approach.

II. THEORY

A. Decomposition of the Initial Supersystem Energy

A major disadvantage of the classical approach is that the fragment charge distributions that it employs, densities translated from infinitely far away to the finite separation cluster geometry, generally do not sum to the total frozen density (with the exception of DEDA[50–52] already discussed in the Introduction). This is because the density corresponding to frozen monomer orbitals (the common choice for the initial supersystem wavefunction) is distorted relative to the simple sum when the fragments overlap. In the overlapping regime, the classical electrostatic energy is thus the coulomb interaction between charge distributions that not only aren't there in the initial state but moreover could possibly never be. We must therefore identify a distinct portion of the frozen electron density that can be justifiably tagged to each monomer: its properly distorted density in the complex.

One way to guarantee that a sum of newly identified fragment densities ($\{\tilde{\rho}_A\}$) will yield a given initial supersystem density (ρ_{init}) is for the new fragment occupied subspace projectors ($\{\tilde{\mathbf{P}}_A\}$) to be orthogonal with a collective span equal to that of the initial supersystem wavefunction ($\mathbf{P}_{init}$). The way that fragment subspaces are chosen initially is of course with energetic optimality in isolation. We propose that the fragment subspaces within the initial supersystem wavefunction be chosen similarly but with a collective energetic optimality condition,

$$E_{frag}^{ortho} = \underset{\{\tilde{\mathbf{P}}_{\alpha,A}\},\{\tilde{\mathbf{P}}_{\beta,A}\}}{\text{minimize}} \sum_A E_A[\tilde{\mathbf{P}}_{\alpha,A}, \tilde{\mathbf{P}}_{\beta,A}] \tag{II.1}$$

and the constraint that they are orthogonal and sum to the initial supersystem density matrix:

$$\text{Tr}\left[\tilde{\mathbf{P}}_{\sigma,A}\mathbf{S}\tilde{\mathbf{P}}_{\sigma,B}\mathbf{S}\right] = \begin{cases} 0 & B \neq A \\ \text{Tr}\left[\tilde{\mathbf{P}}_{\sigma,A}\mathbf{S}\right] & B = A \end{cases} \tag{II.2}$$

$$\mathbf{P}_{\sigma,init} = \sum_A \tilde{\mathbf{P}}_{\sigma,A} \tag{II.3}$$

Each $\tilde{\mathbf{P}}_{\sigma,A}$ has the same rank as the corresponding $\mathbf{P}_{\sigma,A}$ computed for fragment A in isolation.

The new definition of the permanent electrostatic interaction based on this simple optimization problem is then:

$$E_{elec} = \sum_{A<B} \int_{r_1} \int_{r_2} \tilde{\rho}_A^{tot}(\mathbf{r}_1) \frac{1}{\mathbf{r}_{12}} \tilde{\rho}_B^{tot}(\mathbf{r}_2) \tag{II.4}$$

This expression is very similar to the classical expression (I.1); however, unlike in the classical case, this expression can also be written in terms of matrix elements computed from antisymmetric electronic wavefunctions:

$$\begin{aligned} E_{elec} = \quad & \text{Tr}\left[(\mathbf{J}[\mathbf{P}_{init}] + \mathbf{V}_{total})\mathbf{P}_{init}\right] \\ & - \textstyle\sum_A \text{Tr}\left[(\mathbf{J}[\tilde{\mathbf{P}}_A] + \mathbf{V}_A)\tilde{\mathbf{P}}_A\right] + \Delta E_{NN} \end{aligned} \tag{II.5}$$

where ΔE_{NN} is the classical energy change derived from changes in nuclear-nuclear interactions upon formation of the complex.

The orthogonality constraint, (II.2), can be interpreted as inclusion of volume exclusion effects in fragment wavefunction determination. In the interest of lowering the potential

energy of the system via (II.1), each fragment density will be closest to the only nuclei that are known to it, those composing the fragment itself. This density will be partly expelled from the regions of other fragments by the presence of the other fragments' electrons, which are in turn most energetically suited to be near their respective nuclei. The partitioning of the valence space of different fragments is determined by overall energetic importance of that portion of Hilbert space to each fragment. With this volume exclusion interpretation in mind, we put forward the following definition for the "kinetic energy pressure"[18] (KEP) Pauli repulsion term:

$$E_{Pauli}^{KEP} = \sum_A E_A[\tilde{\mathbf{P}}_A] - E_A[\mathbf{P}_A] \tag{II.6}$$

In the complete basis set limit, the KEP energy is a positive semidefinite quantity because the only difference between the two terms in (II.6) is the set of constraints, (II.2), that apply only to the first term.

There are many other possible orthogonal decompositions of the initial supersystem density matrix that could be performed. Two examples are symmetric orthogonalization of the frozen orbitals, or some localization of those orthogonalized orbitals[70]. However, we prefer (II.1) because it uses energetic optimality to associate fragment subspaces with their respective fragment nuclei, the only particles with unambiguous fragment tagging, and it also minimizes what is most often the largest repulsive contribution to the initial interaction energy, (II.6).

The sum of the electrostatic, (II.4), and KEP, (II.6), contributions does not account for the entire frozen energy, (I.3). The remainder is precisely the exchange-correlation (XC) interaction between the properly deformed monomer densities:

$$E_{xc} = E_{XC}[\mathbf{P}_{init}] - \textstyle\sum_A E_{XC}[\tilde{\mathbf{P}}_A] \tag{II.7}$$

$E_{XC}[\mathbf{P}]$ is the chosen XC functional, which is assumed to have at most density matrix dependence (as in Hartree-Fock and local and hybrid density functionals but excluding double-hybrids and post-SCF wavefunction methods). The XC contributions will be divided into two parts, one corresponding to dispersive correlations, and the other corresponding to XC contributions to the Pauli energy.

To identify the dispersive interaction, we subtract the "dispersion-free" part of the interfragment XC interaction from (II.7), which requires evaluation of the same densities using a "dispersion-free" XC (DFXC) functional:

$$E_{disp} = \left(E_{XC}[\mathbf{P}_{init}] - \textstyle\sum_A E_{XC}[\tilde{\mathbf{P}}_A]\right) - \left(E^{DF}_{XC}[\mathbf{P}_{init}] - \textstyle\sum_A E^{DF}_{XC}[\tilde{\mathbf{P}}_A]\right) \tag{II.8}$$

In principle, the problem of finding a DFXC functional to match any given functional has no unique solution since the dispersion interaction itself is not uniquely defined in the overlapping regime. However, in practice there are some plausible options available, reflecting the dispersion-free nature of Hartree-Fock and standard semi-local density functionals, such as revPBE[71]. The former may be natural for functionals that contain a significant fraction of exact exchange, while the latter may be preferable for functionals without exact exchange. The "dispersionless" functional[72] whose name seems appealing for this purpose could also be a candidate; however, it should be kept in mind that this method was trained assuming a SAPT definition of dispersion. Another option is removing a dispersion term from the density functional if that is possible. We think that the additional ambiguity in the method introduced by the non-uniqueness of the DFXC functional is offset by the utility provided by the conceptually significant dispersion term. Regardless, some validation will be necessary.

The interfragment DFXC term that is subtracted in (II.8) is negative semidefinite, and should be dominated by interfragment exchange (it is exactly that when the DFXC functional is taken as Hartree-Fock). Since this exchange effect and Pauli exclusion (given by the "kinetic energy pressure" effect, (II.6)) both result from wavefunction antisymmetrization, we define the full Pauli repulsion term as their sum

$$E_{Pauli} = E^{KEP}_{Pauli} + \left(E^{DF}_{XC}[\mathbf{P}_{init}] - \sum_A E^{DF}_{XC}[\tilde{\mathbf{P}}_A]\right) \tag{II.9}$$

Our overall decomposition of the frozen interaction energy can be expressed as

$$E_{frz} = E_{elec} + E_{Pauli} + E_{disp} \tag{II.10}$$

The new decomposition, (II.10), gives quantum mechanically based numerical values for all three key physical contributions to the frozen interaction. While detailed tests will be

presented in Sec. III, one can anticipate that (II.10) will be most helpful in the regime of weak to moderate fragment overlap, where the Pauli term is not too repulsive and the electrostatic term behaves similarly to classical expectations. However, in the strongly overlapping regime, the Pauli and electrostatic terms can become large in magnitude and opposite in sign, which suggests that they could then be usefully recombined as the dispersion-free frozen energy, $E_{frz}^{DF} = E_{elec} + E_{Pauli}$ to give the alternative decomposition:

$$E_{frz} = E_{frz}^{DF} + E_{disp} \tag{II.11}$$

(II.11) separates only the negative semidefinite (for appropriate functional choices) dispersion term from the full frozen energy.

While the frozen orbital (Heitler-London) wavefunction was mentioned as the initial supersystem wavefunction in the description above, its use is not a requirement. For example, it is also possible to employ an initial wavefunction that has been energy optimized (with a constant density constraint[53]) such as by the removal of constant density polarization[53].

B. Expected Behavior of Terms

When the occupied subspaces of fragments computed in isolation are not overlapping and the basis is sufficiently large such that there is no BSSE, then the orthogonal fragment subspaces that are the solution to (II.1) are precisely the occupied subspaces computed in isolation. This fact guarantees the correct limiting behavior of all terms. For well-separated fragments, the full Pauli repulsion term (II.9) vanishes, and the electrostatic term (II.5) is identical to the classical electrostatic term for equivalently treated fragments and will decay as classical electrostatics predicts. In the short-range, we expect the two components of the Pauli term, KEP and DFXC, to both exhibit exponential decay with intermolecular separation, just as hydrogenic orbital overlap does. In practice, since the magnitude of KEP is significantly larger, the full Pauli term usually turns out to be repulsive, and decays similarly to the KEP term. As the sum of the electrostatic and Pauli terms, the dispersion-free frozen term is evidently repulsive in the compressed region where the latter dominates, and it finally merges with the electrostatic term in the long range because of the rapid decay

of the Pauli term.

As long as the underlying XC functional can describe dispersion interactions, the E_{disp} term should decay as R^{-6} in the long range. At short range, the decay behavior of E_{disp} cannot be predicted, as it will depend on the compatibility between the XC and DFXC functionals, as well as the fact that inter- and intrafragment dynamic correlation effects are not well-separated in the short range. However the short-range behavior will transition smoothly to polynomial R^{-6} decay in the long range if the XC functional permits.

C. Solution of the Optimization Problem for Monomer Subspace Determination

We now turn to the solution of the optimization problem from which the three newly defined EDA terms, E_{elec}, E_{Pauli}, and E_{disp}, follow. The structure of the problem (II.1) is very similar to restricted open shell Hartree-Fock (ROHF) in that only inter-subspace rotations are energetically relevant, and the subspaces are constrained to be orthogonal. For simplicity and without loss of generality we also assume intra-subspace orthogonality. We parametrize the vectors, $\mathbf{T}$, defining the new orthogonal fragment subspaces in terms of orbital rotation parameters, $\mathbf{\Delta}$, as:

$$\mathbf{T} \leftarrow \mathbf{T}\, \mathbf{e}\exp\left(\mathbf{\Delta} - \mathbf{\Delta}^T\right) \tag{II.12}$$

$$\begin{aligned} T^{\mu}_{\bullet\, Ai} \leftarrow \sum_B T^{\mu}_{\bullet\, Bj} \big[\delta_{BjAi} + \Delta_{BjAi} \\ - \Delta_{AiBj} + \tfrac{1}{2} \sum_D (\Delta_{BjDl}\Delta_{DlAi} - \Delta_{BjDl}\Delta_{AiDl} \\ - \Delta_{DlBj}\Delta_{DlAi} + \Delta_{DlBj}\Delta_{AiDl}) + O\left(\mathbf{\Delta}^3\right) \big] \end{aligned} \tag{II.13}$$

$$\tilde{P}^{\mu\nu}_A = T^{\mu}_{\bullet\, Ai} T^{\nu}_{\bullet\, Ai} \tag{II.14}$$

The Taylor series is truncated at 2nd order because only the first and second derivatives of the objective function (II.1) are of interest in this work, and they are both computed at $\mathbf{\Delta} = \mathbf{0}$.

The gradient of the objective function with respect to orbital rotation parameters is thus:

$$\left.\frac{\partial E_{frag}^{ortho}}{\partial \Delta_{CkDl}}\right|_{\mathbf{\Delta}=0} = 2\left[\mathbf{T}^T(\mathbf{F}_D - \mathbf{F}_C)\mathbf{T}\right]_{CkDl} \tag{II.15}$$

where:

$$(F_A)_{\mu\nu} = \frac{\partial E_A[\tilde{\mathbf{P}}_A]}{\partial \tilde{P}_A^{\mu\nu}} \tag{II.16}$$

Iterations for this optimization problem are fairly expensive, requiring number of fragments full Fock matrix builds in the supersystem basis. With this in mind, we now present a preconditioning strategy for this problem that has proven effective within a preconditioned L-BFGS[73–75] algorithm incorporating a robust line search[76]. As in past work[53,54,75], we invert the portion of the Hessian that does not require the evaluation of new two-electron integrals or second functional derivatives of the exchange-correlation energy, which in this case is:

$$\begin{aligned}
&\sum_A \frac{\partial E_{frag}^{ortho}}{\partial \tilde{P}_A^{\mu\nu}} \left.\frac{\partial^2 \tilde{P}_A^{\mu\nu}}{\partial \Delta_{CkDl} \partial \Delta_{XiYj}}\right|_{\mathbf{\Delta}=0} \\
= \;& \left[\mathbf{T}^T(\mathbf{F}_D - 2\mathbf{F}_C + \mathbf{F}_X)\mathbf{T}\right]_{XiDl} \delta_{CkYj} \\
&- \left[\mathbf{T}^T(\mathbf{F}_C - 2\mathbf{F}_D + \mathbf{F}_X)\mathbf{T}\right]_{XiCk} \delta_{DlYj} \\
&+ \left[\mathbf{T}^T(\mathbf{F}_C - 2\mathbf{F}_D + \mathbf{F}_Y)\mathbf{T}\right]_{YjCk} \delta_{DlXi} \\
&- \left[\mathbf{T}^T(\mathbf{F}_D - 2\mathbf{F}_C + \mathbf{F}_Y)\mathbf{T}\right]_{YjDl} \delta_{CkXi}
\end{aligned} \tag{II.17}$$

We compute the inverse of this approximate Hessian applied to a vector iteratively using conjugate gradients, which itself requires only the contraction of (II.17) with a trial vector. This conjugate gradient algorithm is in turn preconditioned with the inverse of an even more approximate form of the Hessian that incorporates only subspace-pair diagonal blocks:

$$\begin{aligned}
&\sum_A \frac{\partial E_{frag}^{ortho}}{\partial \tilde{P}_A^{\mu\nu}} \left.\frac{\partial^2 \tilde{P}_A^{\mu\nu}}{\partial \Delta_{CkDl} \partial \Delta_{CiDj}}\right|_{\mathbf{\Delta}=0} \\
=& -2\left[\mathbf{T}^T(\mathbf{F}_C - \mathbf{F}_D)\mathbf{T}\right]_{CkCi} \delta_{DlDj} \\
&+ 2\left[\mathbf{T}^T(\mathbf{F}_C - \mathbf{F}_D)\mathbf{T}\right]_{DlDj} \delta_{CkCi}
\end{aligned} \tag{II.18}$$

These blocks can be easily inverted after pseudocanonical-like transformations within subspaces. Our guess for the problem (II.1) is the symmetric orthogonalization of the occupied

subspace vectors computed for the fragments in isolation, and it has proven to be a good guess in practice, corresponding to the geometrically optimal instead of the energetically optimal choice for the fragment subspace orthogonalization.

III. RESULTS AND DISCUSSION

A. Computational Details

Calculations in this work were performed with a development version of the Q-Chem software package[77,78]. The initial supersystem wavefunction is the antisymmetric product of monomer wavefunctions (i.e. the Heitler-London or frozen orbital wavefunction), which allows direct comparison of the new approach, (II.10), to the common classical approach, (I.4). For comparison, the total interaction energy is also evaluated as the difference of the fully relaxed SCF energy of the supersystem and the sum of monomer energies. In order to focus on assessing (II.10), polarization and charge transfer contributions are *not* further separated in this work.

To explore the behavior of the newly defined dispersion term, (II.8), we use the ωB97X-V[16] density functional, which includes the VV10[13] non-local correlation (NLC) functional for the treatment of dispersion. ωB97X-V has been shown to perform accurately for many noncovalent interactions[17,79,80]. Since it is a range separated hybrid that includes 100% exact exchange at long-range, Hartree-Fock (HF) is chosen as the most natural choice for the dispersion-free XC (DFXC) functional.

Quadruple-ζ basis sets with diffuse functions are used in this work, including aug-cc-pVQZ[81,82] and def2-QZVPPD[83]. While the results of this decomposition inevitably depend on the employed basis set, we choose these basis sets because they usually converge both the total interaction energy and the frozen energy well, requiring no further corrections for BSSE. Furthermore, our recently developed polarization model has a non-trivial basis set limit for the polarization term and by extension the charge transfer term, enabling the use of large basis sets[54]. The decomposition of the frozen energy presented in this work likewise has a meaningful basis set limit, and a discussion of the basis set convergence of these new terms

for two sample systems, Ne dimer and water-Cl^-, can be found in the supplemental material at URL.[84] For accurate evaluation of interaction energies at long range, unless otherwise specified, the (250, 590) grid (250 radial shells with 590 Lebedev angular points in each) is used to compute the exchange-correlation energy, while (75, 302) is used for the VV10 NLC functional.

Unless otherwise noted, the coordinates investigated correspond to the rigid displacement of monomers relative to the ωB97X-V/aug-cc-pVQZ equilibrium structure. No corrections for BSSE were performed in this work. While our new method applies to an arbitrary number of fragments as well as the many-body expansion thereof, we restrict ourselves to dimer applications where chemical intuition is strongest and the distance-dependence of each term can be easily manifested.

B. Neon dimer

To validate our frozen decomposition scheme, especially the tentative choice of HF for the DFXC functional, we first investigate the Ne dimer whose long-range interaction is entirely dispersion. Indeed, the binding is almost completely due to the frozen energy. Due to the grid sensitivity of this particular system, we upgrade the grid for the XC functional to (500, 974) and the grid for the non-local correlation functional to (99, 590).

Figure 1 shows how the frozen energy (black) is decomposed into three terms based on the new scheme (solid) and two terms based on the classical scheme (dashed). A sharp contrast between these two schemes can be observed. The classical Pauli term transitions to attractive at 2.85Å separation, even shorter than the 3.0Å equilibrium distance, which is in essence incorrect. By contrast, the Pauli repulsion contribution evaluated by the new scheme stays repulsive in the entire region. The classical electrostatic term is slightly attractive, and rapidly decays to near zero for R$>$ 3.0Å. The electrostatic contribution evaluated by the new scheme, however, is surprisingly attractive.

To understand the results for the electrostatics, we plot the differences in the fragment densities that are used to compute the new and classical electrostatic terms in Figure 2. This plot displays the characteristic density deformations that occur upon formation of the

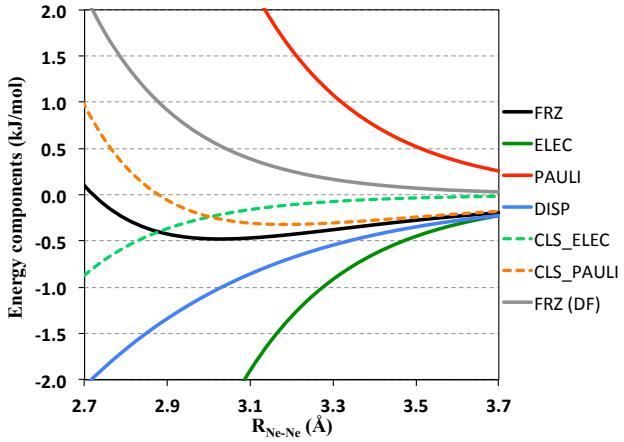

FIG. 1: Decomposition of the ωB97X-V/aug-cc-pVQZ frozen energy (FRZ) for the Ne dimer based on the new method ((II.10) and (II.11): ELEC, PAULI, DISP, FRZ(DF)) compared with the classical approach ((I.4): CLS_ELEC, CLS_PAULI).

antisymmetric product of monomer wavefunctions that have been discussed by others[21]. Density is depleted from the region between the monomers and increased near the nuclei. Since we have divided the initial supersystem wavefunction into monomer contributions, we are able to visualize the deformation in each monomer. Figure 2 clearly reveals that each fragment develops density close to the nuclei of the other, and this significant charge penetration effect is the key origin of the attractive electrostatics at short-range. This charge penetration effect is likely a consequence of the orthogonality constraint, (II.2).

To verify this, we compute the deformed fragment densities using two alternative schemes: (1) using symmetrically orthogonalized isolated fragment MOs (the old fragment tags still hold after orthogonalization) to construct $\tilde{\mathbf{P}}_\mathbf{A}$ for each fragment (the initial guess used in optimizing (II.1)–(II.3)); (2) using the orthogonalized fragment densities that maximize their self-repulsion energies, which is essentially performing Edmiston-Ruedenberg (ER) localization for fragment densities[85]. In the second case, the original objective function (II.1) is replaced by

$$E^{ortho}_{J,frag} = \max_{\{\tilde{\mathbf{P}}_{tot,A}\}} \sum_A \sum_{\mu\nu\lambda\sigma} \tilde{P}^{\mu\nu}_{tot,A}(\mu\nu|\lambda\sigma)\tilde{P}^{\lambda\sigma}_{tot,A} \tag{III.1}$$

where $\tilde{\mathbf{P}}_{\mathbf{tot,A}} = \tilde{\mathbf{P}}_{\alpha,\mathbf{A}} + \tilde{\mathbf{P}}_{\beta,\mathbf{A}}$ and the constraints, (II.2) and (II.3), still apply.

The resulting electrostatic energies evaluated using (II.5) are plotted in Figure 3 for all

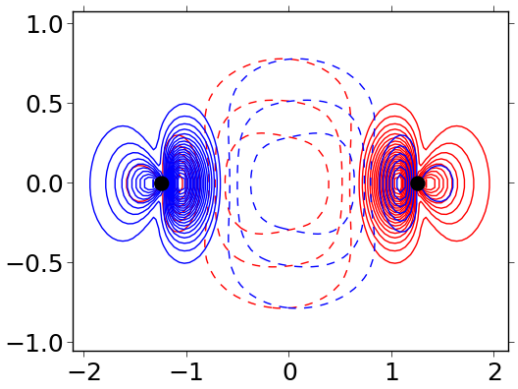

FIG. 2: Contour plot of the change in ωB97X-V/aug-cc-pVQZ density for two interacting Ne atoms, at $R_{\text{Ne-Ne}} = 2.5$Å. Values plotted are the differences in the total electron density, integrated to a plane ($\Delta\rho_A(x,y) = \int \mathrm{d}z \Delta\rho_A(x,y,z)$), for each fragment, A, upon going from the optimal isolated fragment density matrix to that of the fragment in the initial supersystem wavefunction ($\tilde{\mathrm{P}}_A$). Contours are evenly spaced at 0.01 $\mathrm{e}^-/\text{Å}^3$ with positive contours (density enhanced) solid and negative contours (density depleted) dashed. Dots indicate the positions of nuclei.

four definitions. Despite their different choices for the objective function, all schemes with the orthogonality constraint enforced yield a considerably more attractive electrostatics term compared to the classical scheme. Only minimal differences exist between them, and the objective function based on energetic optimality, (II.1), gives slightly less attractive results than its alternatives, mainly because of its variationally minimized kinetic energy pressure term. We hence conclude that the more attractive electrostatic term in the new scheme originates from the constraint of partitioning the initial supersystem density matrix into strictly orthogonal fragment densities. It does not seem that fragment subspaces meeting these criteria can be constructed without such density tails.

While robust to its exact definition as established above, the new electrostatics term does behave counterintuitively, both in terms of distance dependence and magnitude, when the density distortions that are a consequence of electron antisymmetry are large. We thus alternatively report the dispersion-free frozen term defined as the sum of E_{elec} and E_{Pauli}

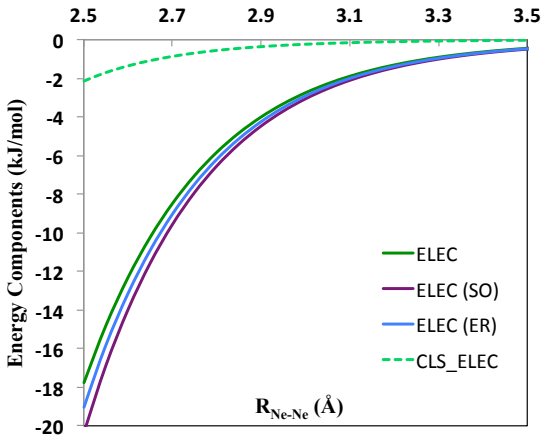

FIG. 3: The contribution of electrostatics to the Ne dimer interaction evaluated based on equation (II.4), with fragment densities that are (i) fully optimized based on (II.1)–(II.3) (solid green), (ii) localized with an Edmiston-Ruedenberg (ER) scheme (blue), (iii) symmetrically orthogonalized (SO) (violet), in the strongly interacting region (2.5Å–3.5Å). Values evaluated with the classical scheme are also plotted (dashed green) for comparison.

in these scenarios (the grey curve in Figure 1). It is repulsive in the plotted region but not nearly as strongly as the new Pauli term. In this neon dimer case, it roughly corresponds to the repulsive van der Waals (vdW) component of classical force fields.

Dispersion is not separated in the classical scheme and thus contributes to the classical Pauli term. By contrast, in the new scheme, with the assistance of DFXC, the attractive dispersion contribution is separated out (as the light blue curve in Figure 1). The long-distance R^{-6} asymptotic behavior of the new dispersion term is confirmed by the log-log plot from 5Å to 10Å in Figure 4b. The decaying behavior of new and classical Pauli terms, as well as the FRZ(DF) term and the attractive electrostatic term discussed above, are displayed in Figure 4a ($\log E$ vs. R). The new Pauli and electrostatic terms exhibit almost synchronous exponential decay although they have opposite signs, which further confirms the necessity of using the FRZ(DF) term (it decays exponentially when $R < 4.5$Å as well) in this case. On the other hand, the classical Pauli term only shows exponential decay at compressed distances due to its contamination by what are truly dispersion interactions at

greater separations.

Overall, the energy components of the frozen energy computed by the new scheme behave as anticipated in Sec. II B. Choosing Hartree-Fock as the DFXC functional is evidently compatible with the dispersion-corrected range-separated hybrid ωB97X-V functional employed here.

C. Ammonia Borane

The strongly interacting ammonia borane complex is dominated by the non-frozen contributions: induced electrostatics and charge transfer. Nonetheless, its frozen interaction is of interest because both monomers have permanent dipole moments, which make a considerable contribution to the interaction energy. Also, with a rather short value of R_e (1.65Å), and thus large inter-monomer overlap, there may be interesting differences between the new and classical frozen energy decompositions.

The decomposition of the frozen orbital interaction by both the new and classical schemes is shown in Figure 5. The energy scales are large due to the strength of the interaction at the distances considered. On this scale, the magnitude of the dispersion contribution is relatively small. As a result, the dispersion-free frozen term, FRZ(DF), differs only minimally from the frozen energy to be decomposed. Most strikingly, relative to the classical model, the new scheme again offers a qualitatively different description of the permanent electrostatic interaction at compressed distances. Opposite to the Ne dimer case, the new electrostatic term is less attractive by 150 kJ/mol at $R_{N\text{-}B}$=1.65Å and becomes repulsive at highly compressed distances ($R_{N\text{-}B}$=1.00Å) while the classical electrostatic term is still becoming more attractive upon compression at that separation.

To better understand the origin of this dramatic difference in evaluated permanent electrostatics, we plot the change in the fragment densities (Figure 6) just as in the previous example. While there is some increase in ammonia density (red) near the borane nuclei due to the orthogonalization tails, the major effect is relocation of ammonia charge from near the boron nucleus to a region much closer to the nitrogen atom, resulting in greatly diminished charge interpenetration and increased shielding of nuclei relative to the classical

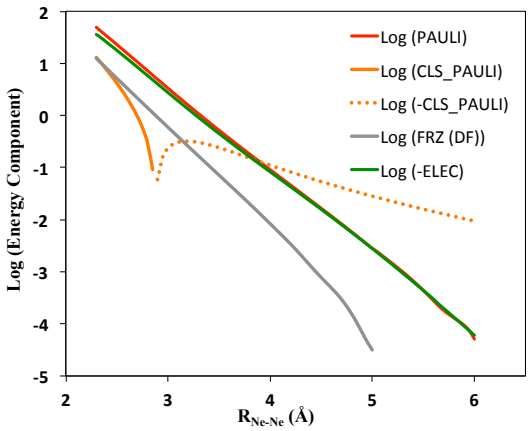

(a) Plot of $\log(\pm E)$ vs. $R_{\text{Ne-Ne}}$ (2.3–6.0Å) for the Pauli term evaluated by the newly introduced and classical approaches. Least-squares fits show that E_{Pauli} and E_{frz}^{DF} show exponential decay with distance. The classical Pauli term changes sign due to being contaminated with dispersion.

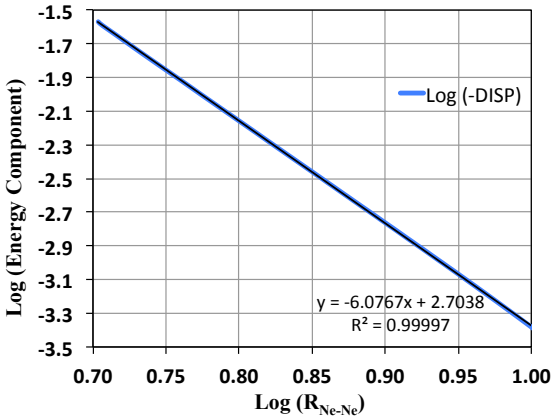

(b) Plot of $\log(-E)$ vs. $\log(R_{\text{Ne-Ne}})$ (5.0-10.0Å) for the dispersion term computed by the new scheme. A least-square fit establishes R^{-6} asymptotic behavior in the long range.

FIG. 4: An assessment of the long-range decay of EDA terms computed with ωB97X-V/aug-cc-pVQZ for the Ne dimer. Terms that are not uniformly signed throughout the coordinate are split into attractive(-) and repulsive(+) portions.

approach. The result is thus an overall diminished electrostatic interaction. Because the classical electrostatic interaction is considerably more attractive, the corresponding classical

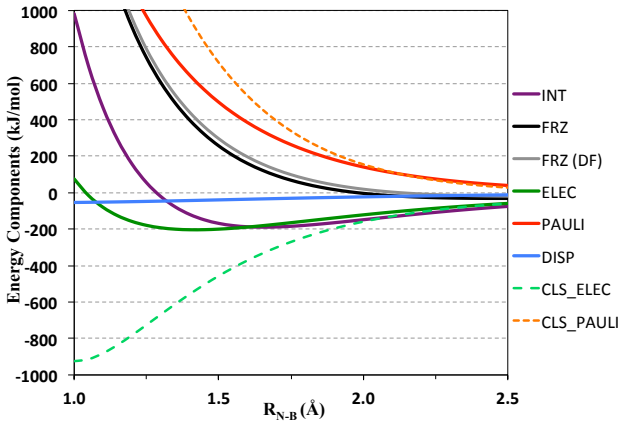

FIG. 5: Decomposition of the frozen energy for the rigid dissociation of the ammonia borane complex along the N-B coordinate, relative to the ωB97X-V/aug-cc-pVQZ optimized geometry (with C_{3v} symmetry, equilibrium $R_{\text{N-B}} = 1.65$Å). Energy terms evaluated by the new scheme (ELEC, PAULI, DISP, FRZ(DF)) and the classical approach (CLS_ELEC, CLS_PAULI) are compared.

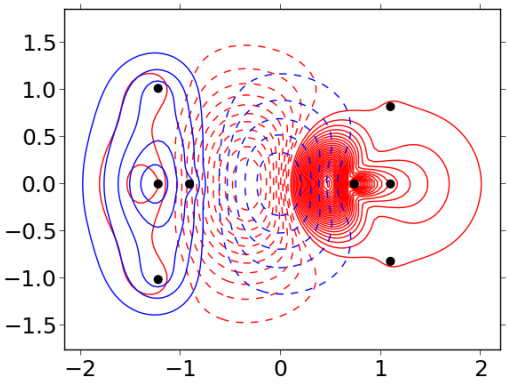

FIG. 6: Contour plot of the change in density for NH_3 (red) and BH_3 (blue) in the ωB97X-V/aug-cc-pVQZ optimized ammonia borane complex rigidly translated to $R_{\text{N-B}} = 1.65$Å (near R_e). Contours are evenly spaced at 0.2 $e^-/Å^3$, and other details are as in Figure 2.

Pauli repulsion term is also much larger in magnitude despite its inclusion of dispersion contributions to binding.

Through this case, we see that the relative magnitudes of the new and classical electrostatics terms are affected by two factors with opposite consequences: the localization of fragment electron densities (more shielded nuclei and diminished charge interpenetration), and the formation of orthogonalization tails near the nuclei on other fragments (enhanced interfragment nuclei-electron attraction). The interplay of these two factors can lead to very different outcomes in different chemical systems, as we see in comparing ammonia borane to the neon dimer.

D. Water-Na^+

The decomposition of the frozen energy for water interacting with Na^+ as a function of rigidly dissociating the complex along the $R_{O\text{-}Na}$ coordinate appears in Figure 7. The binding is dominated by the frozen term, especially the contribution of permanent electrostatics, which is the primary attractive interaction near equilibrium and beyond. Dispersion is relatively insignificant as expected. By contrast with Ne_2 and ammonia borane, there is only a slight difference in the new and classical electrostatic terms around R_e (13 kJ/mol at $R_{O\text{-}Na} = 2.25$Å). The difference between these two terms increases to a maximum of only 43 kJ/mol (or about 20% of the magnitude of the new electrostatics) at 1.70Å.

The differences in the densities used to compute the new and classical electrostatic terms appear in Figure 8. We note that the density difference contours are drawn at intervals of one quarter the size compared to those used for ammonia borane above. There is diminished density distortion in this cationic system with its fairly compact density due to less inter-monomer occupied orbital overlap. Again, density is generally relocated from the inter-monomer region closer to the nuclei with some tails developing near other nuclei. The increase in sodium density (red) both near the oxygen atom of water (blue) as well as on the opposite side of the sodium atom from water (the Na nucleus is less shielded) may be the reason for a more favorable electrostatic interaction energy as computed by the new scheme around the equilibrium separation. The decrease in the difference between the two

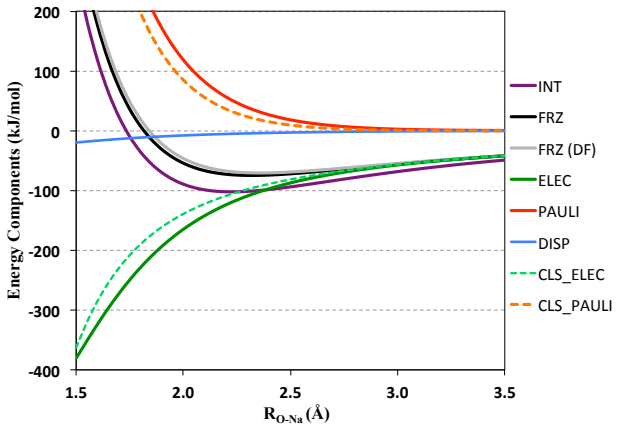

FIG. 7: Decomposition of the frozen energy (FRZ) for the rigid dissociation of H_2O-Na^+ complex along the O-Na coordinate, relative to the ωB97X-V/aug-cc-pVQZ optimized geometry (with C_{2v} symmetry, equilibrium $R_{O\text{-}Na} = 2.23$Å). Energy terms evaluated by the new scheme (ELEC, PAULI, DISP) and the classical approach (CLS_ELEC, CLS_Pauli) are compared.

electrostatic energies for very compressed geometries can be seen as the negation of this effect by the generally less extended electron density in the new scheme relative to the classical approach.

Due to the minimal distortion of the density in the supersystem relative to the isolated subsystems, the differences in the new and classical Pauli repulsion terms are likewise not appreciable, with approximately half of the difference in the short range and the entire difference in the long range explained by the presence of dispersion interactions in the classical term. For this reason, to report the combination of the electrostatic and Pauli energies here turns out to be rather unnecessary. Plots of the asymptotic distance dependence of electrostatics show the expected R^{-2} charge-dipole behavior, and the characteristic R^{-6} decay of the new dispersion term. See supplemental material at URL for more information on these plots.[86]

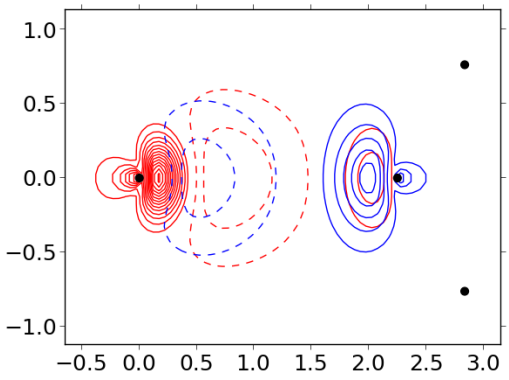

FIG. 8: Contour plot of the change in density for Na^+ (red) and H_2O (blue) in the ωB97X-V/aug-cc-pVQZ optimized water sodium cation complex rigidly translated to $R_{O\text{-}Na}$ = 2.25Å. Contours are evenly spaced at 0.05 $e^-/Å^3$, and other details are as in Figure 2.

E. Water-Cl^-

The water-Cl^- complex contains an anion with a considerably more diffuse density than that in the cationic system investigated above. Hence we expect a larger deviation from the decomposition produced by the classical approach due to the greater inter-fragment occupied orbital overlap and thus greater density distortion upon formation of the frozen wave function. The decomposition of the frozen energy for this system rigidly dissociated along the H-Cl coordinate is shown in Figure 9. The comparatively bigger difference between the frozen energy and the total interaction indicates increased importance of polarization and charge transfer in this case relative to the cationic system investigated above. However, the frozen interaction is still the most favorable at equilibrium and beyond.

In the long range (roughly > 2.5Å), electrostatics accounts for most of the binding interaction via both new and classical schemes. In Figure 9, we see that indeed the electrostatic terms differ more in this diffuse system than for water-Na^+, especially when one considers the reduced scale of the total interaction energy. Near R_e, the electrostatic terms differ by about 40 kJ/mol (at 2.15Å). They differ by a maximum of 66 kJ/mol (about 40% of the classical electrostatics) near 1.65Å.

The fact that the new electrostatic term is more attractive in the overlapping regime

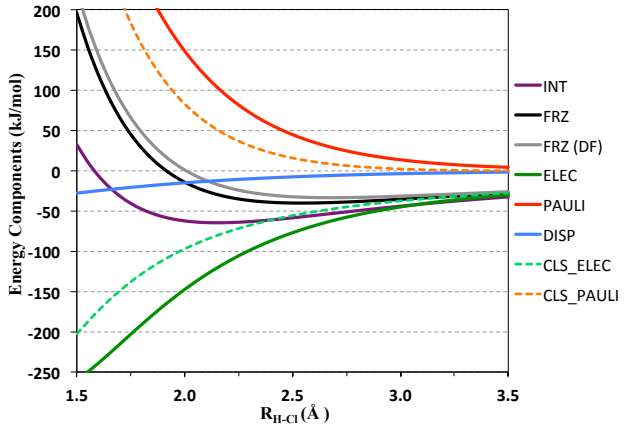

FIG. 9: Decomposition of the frozen energy (FRZ) for the rigid dissociation of H_2O-Cl^- complex along the H-Cl coordinate, relative to the ωB97X-V/aug-cc-pVQZ optimized geometry (with C_s symmetry, equilibrium $R_{H\text{-}Cl} = 2.15$Å). Energy terms evaluated by the new decomposition scheme (ELEC, PAULI, DISP) and the classical approach (CLS_ELEC, CLS_Pauli) are compared.

is due to the fragment density changes occurring on formation of the initial supersystem wavefunction as illustrated in Figure 10. The usual density depletion in the inter-fragment region occurs; however, the water density (blue) primarily increases between the hydrogen (the one closer to Cl^-) and oxygen atoms, leaving the proton generally less shielded from the anion. Again, the difference between them decreases at very compressed geometries where the new electrostatic term becomes less attractive faster due to the different treatment of the interpenetration of charge in the two methods.

As in the water–Na^+ case, the Pauli term computed by the new scheme turns out to be more repulsive at all separations, and the maximum difference takes place at 1.6Å (90 kJ/mol). Approximately half of the difference in Pauli repulsion terms at short and mid range and the entire difference in the long range is caused by the inclusion of dispersion in the classical Pauli term. The enhanced contribution of dispersion to the total binding compared to the former case is also characterized by Figure 9. The dispersion-free frozen term correspondingly differs more with respect to the entire frozen energy than it did in the water–Na^+ case.

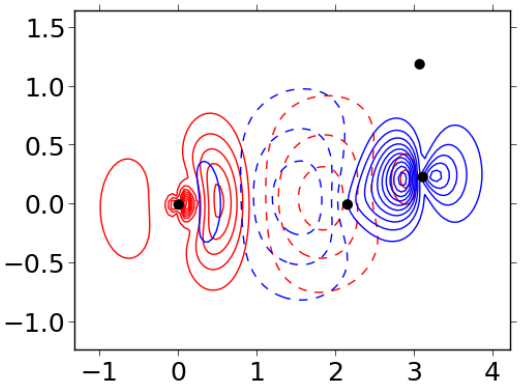

FIG. 10: Contour plot of the change in density for Cl^- (red) and H_2O (blue) in the ωB97X-V/aug-cc-pVQZ optimized water chloride complex rigidly translated to the essentially equilibrium $R_{H\text{-}Cl} = 2.15$Å. Contours are evenly spaced at 0.1 $e^-/Å^3$, and other details are as in Figure 2.

F. Naphthalene Dimer

The naphthalene dimer has several low-lying conformations[87,88], including the parallel displaced and T-shaped conformers illustrated in Figure 11. In this section we compare the new and classical decompositions of the frozen interaction energy (which dominates the total interaction energy) for these two naphthalene dimer configurations as a function of rigid translation of the monomers inwards and outwards from their equilibrium geometries.

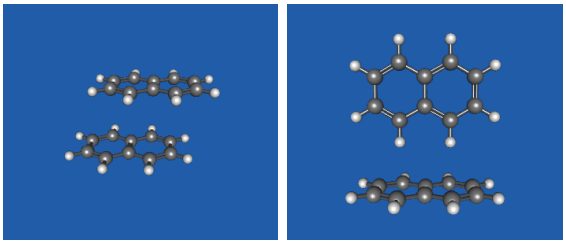

FIG. 11: Equilibrium geometries of naphthalene dimer with two configurations (left: parallel-displaced; right: T-shaped)

Figure 12 shows ωB97X-V/def2-QZVPPD results for the parallel-displaced naphthalene dimer (displacements away from $R_e = 3.51$Å) using the geometry from Ref. 88. The (99, 590)

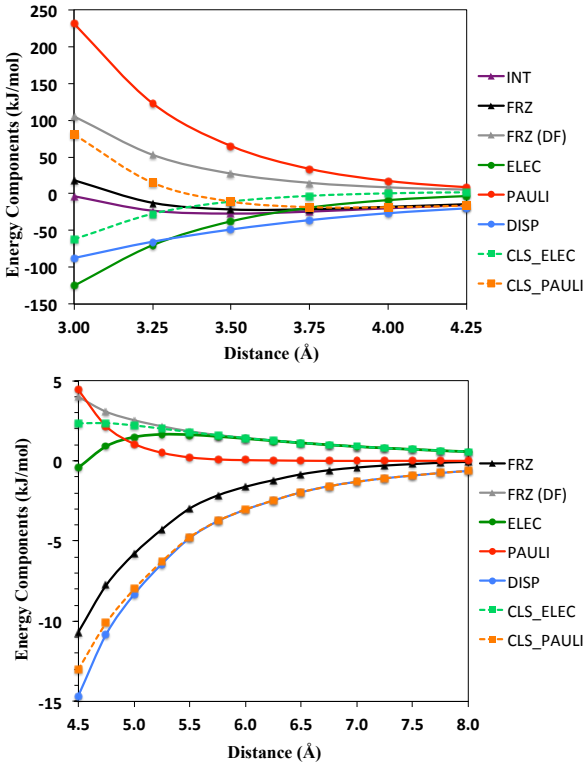

FIG. 12: Decomposition of the frozen energy for the rigid dissociation of the parallel-displaced naphthalene dimer. The intermolecular separation is measured by the interplanar distance. Upper: short-range (3.0–4.25Å); Lower: long-range (4.5–8.0Å).

and SG-1[89] grids were used to integrate the XC and NLC functionals, respectively. Terms in the short range and long range are plotted separately with different energy scales to show the long range with adequate resolution. The frozen interaction is the largest contribution to the binding energy at all separations, while the non-frozen components gain somewhat increased importance in the compressed region.

Let us first consider the long-range (lower panel of Figure 12). The new frozen energy decomposition reveals that the dispersion interaction is the most important stabilizing force. The value of the new scheme is clear since inspecting the long range (lower panel) shows that the classical Pauli is entirely dispersion, while the new Pauli term behaves qualitatively correctly. Electrostatics at long-range (> 4.75Å) are repulsive by both new and old schemes, corresponding to an unfavorable quadrupole-quadrupole (Q-Q) interaction, and

the dispersion-free frozen interaction approaches this limit also. Since the Q-Q interaction decays more slowly (R^{-5}) than dispersion, at $R > 10$Å (beyond the plotted region), its magnitude becomes larger than dispersion (+0.26 vs. −0.19 kJ/mol), and thus the net interaction becomes repulsive.

In the short-range (upper panel of Figure 12), the new electrostatic contribution is significantly more attractive than its classical counterpart, which has also become net attractive. As for the Ne dimer, discussed previously, the difference is most exaggerated at the most compressed distances where density deformations upon the formation of the frozen wavefunction are largest. On the other hand, the dispersion-free frozen term in the overlapping regime gives a moderately repulsive potential, which seems to be a reasonable estimator for the effective van der Waals interaction in models where electrostatics are assumed to be zero (i.e. as might be the case in some simple force fields).

Results for the T-shaped configuration of the naphthalene dimer (Figure 11, right) are shown in Figure 13, as a function of displacement away from the equilibrium geometry ($R_e \sim 5$Å defined as the centroid distance between two monomers) from Ref. 90. Since fewer atoms are in close contact in this configuration, at equilibrium we see diminished magnitudes of both the short-range repulsion (characterized by the dispersion-free frozen term) and dispersion compared to the parallel-displaced case. Thus despite favorable electrostatics, the net effect is slightly weaker binding at equilibrium.

The long-range electrostatics for the T-shaped configuration turns out to be attractive, which can also be understood from the electrostatic potential around the naphthalene molecule. At 10Å separation, the attractive permanent electrostatics and the dispersion interaction contribute almost equally to the binding (E_{elec}= -0.24 kJ/mol, E_{disp}= -0.28 kJ/mol). Their combined effect makes the T-shaped configuration more strongly bound than the parallel-displaced naphthalene dimer at large intermolecular separations, although it is less favorable at equilibrium.

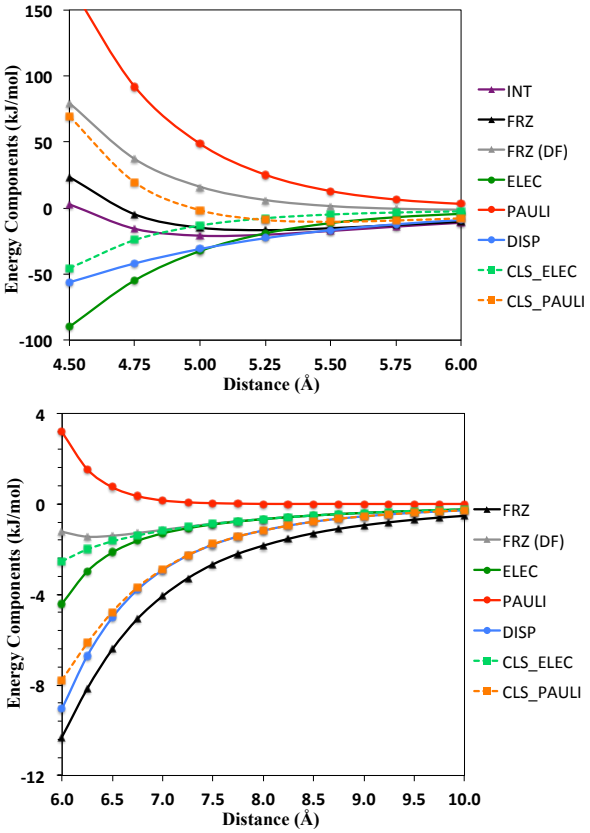

FIG. 13: Decomposition of the frozen energy for the rigid dissociation of the T-shaped naphthalene dimer. The intermolecular separation is measured by the centroid distance between two monomers. Upper: short-range (4.5–6.0Å); Lower: long-range (6.0–10.0Å).

IV. DISCUSSION AND CONCLUSIONS

In this work, we have presented a new scheme, (II.10), for the identification of permanent electrostatic, Pauli repulsion, and dispersion contributions to binding in Kohn-Sham density functional theory calculations of intermolecular interactions. Together these terms make up the "frozen" interaction which excludes the polarization and charge transfer effects of the total interaction. A notable difference between this scheme and what we have termed the classical approach is that antisymmetric electronic wavefunctions are used for the evaluation of all terms. This is accomplished by identifying fragment contributions to the initial supersystem wavefunction based on a constrained sum-of-fragments energetic optimality cri-

terion. Dispersion is disentangled from other exchange-correlation (XC) effects with the aid of a dispersion free XC (DFXC) functional, via (II.8).

We have presented a series of numerical examples that compare results from the new decomposition against those from the classical scheme for Ne_2, NH_3-BH_3, H_2O-Na^+, H_2O-Cl^-, and the naphthalene dimer, $(C_{10}H_6)_2$. These calculations used the ωB97X-V density functional, together with Hartree-Fock (HF) as the DFXC functional. This combination yields very reasonable dispersion energies for all examples tested, though there are other alternatives. The simplest one is to set the DFXC to zero, in which case the dispersion term becomes the interfragment XC energy, and dispersion is not separated. Another possibility is to simply remove the VV10 component of the ωB97X-V functional to define DFXC. Further study is needed to recommend a DFXC functional for other primary functionals, even for those that add a simple damped C_6 potential (i.e. the -D or -D3 type). In the latter case, the uncorrected functional itself might serve as the DFXC functional. However, the damping of their contributions in the overlapping regime where interfragment dynamic correlation is important suggests that testing is still necessary.

The new electrostatic term matches the classical electrostatic term in the non-overlapping regime, but they differ intriguingly in the overlapping regime, with the ordering depending on system-specific density deformations associated with the new term. For two dispersion-bound complexes, the neon dimer and naphthalene dimer, a very interesting result is that the new electrostatic term is strongly attractive in the overlapping regime, decaying roughly exponentially with overlap. Detailed analysis for Ne_2 shows that this is a consequence of the orthogonality constraint imposed on the fragment densities, which permits significant charge penetration from one fragment to nuclei of the other.

The sum of the new electrostatics and the new Pauli repulsion is also used to define a dispersion-free frozen energy, E_{frz}^{DF}. It is worthwhile to examine E_{frz}^{DF} because both the new and classical electrostatic terms can behave in counterintuitive ways in the strongly overlapping regime. Examples such as Ne_2, $(C_{10}H_6)_2$ and NH_3-BH_3 fall into this category. E_{frz}^{DF} can be interpreted as an effective van der Waals interaction (incorporating electrostatics).

The new Pauli repulsion term, (II.9), consists of a positive semidefinite kinetic energy pressure term, which is variationally minimized, plus interfragment DFXC interactions, which

are negative semi-definite. In the examples presented, the new Pauli repulsion is overall positive, and it decays roughly exponentially as expected. By contrast, the classical Pauli term includes contributions from what we have separated out as the dispersion term, which causes the classical Pauli term to become attractive and describe dispersive interactions in the long range.

In summary, with the dramatic advances in density functionals for accurate treatment of non-covalent interactions[7,16,17], it is important that energy decomposition analysis can separate the three contributions of the frozen interaction, permanent electrostatics, Pauli repulsion, and attractive dispersion interactions. The new approach proposed and tested here provides a useful contribution towards this goal. It may also aid in the development of classical force fields (both functional forms and specific parameters) based on accurate density functional theory calculations.

V. ACKNOWLEDGMENTS

This work was supported by a grant (CHE-1363342) from the U.S. National Science Foundation.

REFERENCES

[1]B. Jeziorski, R. Moszynski, and K. Szalewicz, Chem. Rev. **94**, 1887 (1994).

[2]A. J. Stone, *The Theory of Intermolecular Forces* (Oxford University Press, Oxford, 2013).

[3]A. E. Reed, L. A. Curtiss, and F. Weinhold, Chem. Rev. **88**, 899 (1988).

[4]M. von Hopffgarten and G. Frenking, WIRES Comput. Mol. Sci. **2**, 43 (2012).

[5]Y. Mo, P. Bao, and J. Gao, Phys. Chem. Chem. Phys. **13**, 6760 (2011).

[6]M. J. S. Phipps, T. Fox, C. S. Tautermann, and C.-K. Skylaris, Chem. Soc. Rev. **44**, 3177 (2015).

[7]J. Klimes and A. Michaelides, J. Chem. Phys. **137**, 120901 (2012).

[8]R. A. DiStasio Jr., V. V. Gobre, and A. Tkatchenko, J. Phys.: Condens. Matter **26**, 213202 (2014).

[9]C. Corminboeuf, Acc. Chem. Res. **47**, 3217 (2014).

[10]J. P. Wagner and P. R. Schreiner, Ang. Chem. Int. Ed. **54**, 12274 (2015).

[11]S. Grimme, J. Comput. Chem. **27**, 1787 (2006).

[12]S. Grimme, J. Antony, S. Ehrlich, and H. Krieg, J. Chem. Phys. **132**, 154104 (2010).

[13]O. A. Vydrov and T. Van Voorhis, J. Chem. Phys. **133**, 244103 (2010), arXiv:1009.1421.

[14]K. Berland, V. R. Cooper, K. Lee, E. Schroeder, T. Thonhauser, P. Hyldgaard, and B. I. Lundqvist, Rep. Prog. Phys. **78**, 066501 (2015).

[15]J. D. Chai and M. Head-Gordon, Phys. Chem. Chem. Phys. **10**, 6615 (2008).

[16]N. Mardirossian and M. Head-Gordon, Phys. Chem. Chem. Phys. **16**, 9904 (2014).

[17]N. Mardirossian and M. Head-Gordon, J. Chem. Phys. **142** (2015).

[18]V. F. Weisskopf, Science **187**, 605 (1975).

[19]J. Thirman and M. Head-Gordon, J. Phys. Chem. Lett. **5**, 1380 (2014).

[20]P. R. Horn, E. J. Sundstrom, T. A. Baker, and M. Head-Gordon, J. Chem. Phys. **138**, 134119 (2013).

[21]F. M. Bickelhaupt and E. J. Baerends, in *Reviews in Computational Chemistry*, Vol. 15, edited by K. B. Lipkowitz and D. B. Boyd (John Wiley & Sons, Inc., New York, 2007) Chap. 1, pp. 1–86.

[22]A. Krapp, F. M. Bickelhaupt, and G. Frenking, Chem. Eur. J. **12**, 9196 (2006).

[23]K. Kitaura and K. Morokuma, Int. J. Quantum Chem. **10**, 325 (1976).

[24]K. Morokuma, Acc. Chem. Res. **10**, 294 (1977).

[25]W. Chen and M. S. Gordon, J. Phys. Chem. **100**, 14316 (1996).

[26]P. Reinhardt, J.-P. Piquemal, and A. Savin, J. Chem. Theory Comput. **4**, 2020 (2008).

[27]M. Mandado and J. M. Hermida-Ramón, J. Chem. Theory Comput. **7**, 633 (2011).

[28]K. Yamada and N. Koga, Theor. Chem. Acc **131**, 1178 (2012).

[29]T. Ziegler and A. Rauk, Theor. Chem. Acc **46**, 1 (1977).

[30]T. Ziegler and A. Rauk, Inorg. Chem. **18**, 1558 (1979).

[31]M. P. Mitoraj, A. Michalak, and T. Ziegler, J. Chem. Theory Comput. **5**, 962 (2009).

[32]S. Ndambuki and T. Ziegler, Int. J. Quantum Chem. **113**, 753 (2013).

[33]S. Rybak, B. Jeziorski, and K. Szalewicz, J. Chem. Phys. **95**, 6576 (1991).

[34]A. J. Misquitta, B. Jeziorski, and K. Szalewicz, Phys. Rev. Lett. **91**, 033201 (2003).

[35]A. J. Misquitta, R. Podeszwa, B. Jeziorski, and K. Szalewicz, J. Chem. Phys. **123**, 214103 (2005).

[36]I. C. Hayes and A. J. Stone, Mol. Phys. **53**, 83 (1984).

[37]P. S. Zuchowski, R. Podeszwa, R. Moszyski, B. Jeziorski, and K. Szalewicz, J. Chem. Phys. **129**, 084101 (2008).

[38]A. J. Stone and A. J. Misquitta, Chem. Phys. Lett. **473**, 201 (2009).

[39]A. J. Misquitta, J. Chem. Theory Comput. **9**, 5313 (2013).

[40]Y. Mo, J. Gao, and S. D. Peyerimhoff, J. Chem. Phys. **112**, 5530 (2000).

[41]Y. Mo, L. Song, and Y. Lin, J. Phys. Chem. A **111**, 8291 (2007).

[42]S. N. Steinmann, C. Corminboeuf, W. Wu, and Y. Mo, J. Phys. Chem. A **115**, 5467 (2011).

[43]D. G. Fedorov and K. Kitaura, J. Comput. Chem. **28**, 222 (2007).

[44]M. C. Green, D. G. Fedorov, K. Kitaura, J. S. Francisco, and L. V. Slipchenko, J. Chem. Phys. **138**, 074111 (2013).

[45]J. Kong, Z. Gan, E. Proynov, M. Freindorf, and T. R. Furlani, Phys. Rev. A **79**, 042510 (2009).

[46]S. N. Steinmann and C. Corminboeuf, J. Chem. Theory Comput. **6**, 1990 (2010).

[47]P. Su and H. Li, J. Chem. Phys. **131**, 014102 (2009).

[48]P. Su, H. Liu, and W. Wu, J. Chem. Phys. **137**, 034111 (2012).

[49]P. Su, Z. Jiang, Z. Chen, and W. Wu, J. Phys. Chem. A **118**, 2531 (2014).

[50]Q. Wu, P. W. Ayers, and Y. Zhang, J. Chem. Phys. **131**, 164112 (2009).

[51]Z. Lu, N. Zhou, Q. Wu, and Y. Zhang, J. Chem. Theory Comput. **7**, 4038 (2011).

[52]Q. Wu, J. Chem. Phys. **140**, 244109 (2014).

[53]P. R. Horn and M. Head-Gordon, Submitted to J. Chem. Phys. (2015).

[54]P. R. Horn and M. Head-Gordon, J. Chem. Phys. **143**, 114111 (2015).

[55]E. D. Glendening and A. Streitwieser, J. Chem. Phys. **100**, 2900 (1994).

[56]G. K. Schenter and E. D. Glendening, J. Phys. Chem. **100**, 17152 (1996).

[57]E. D. Glendening, J. Phys. Chem. A **109**, 11936 (2005).

[58]A. Reed and F. Weinhold, J. Chem. Phys. **78**, 4066 (1983).

[59]J. K. Badenhoop and F. Weinhold, J. Chem. Phys. **107**, 5406 (1997).

[60]J. K. Badenhoop and F. Weinhold, J. Chem. Phys. **107**, 5422 (1997).

[61]J. K. Badenhoop and F. Weinhold, Int. J. Quantum Chem. (1998).

[62]P. De Silva and J. Korchowiec, J. Comput. Chem. **32**, 1054 (2011).

[63]S. Liu, J. Chem. Phys. **126**, 244103 (2007).

[64]D. Fang, J.-P. Piquemal, S. Liu, and G. A. Cisneros, Theor. Chem. Acc **133**, 1484 (2014).

[65]W. J. Stevens and W. H. Fink, Chem. Phys. Lett. **139**, 15 (1987).

[66]P. . S. Bagus, K. Hermann, and C. W. J. Bauschlicher, J. Chem. Phys. **80**, 4378 (1984).

[67]R. Z. Khaliullin, M. Head-Gordon, and A. T. Bell, J. Chem. Phys. **124**, 204105 (2006).

[68]R. Z. Khaliullin, E. A. Cobar, R. C. Lochan, A. T. Bell, and M. Head-Gordon, J. Phys. Chem. A **111**, 8753 (2007).

[69]R. Z. Khaliullin, A. T. Bell, and M. Head-Gordon, J. Chem. Phys. **128**, 184112 (2008).

[70]J. E. Subotnik, A. Sodt, and M. Head-Gordon, Phys. Chem. Chem. Phys. **9**, 5522 (2007).

[71]Y. Zhang and W. Yang, Phys. Rev. Lett. **80**, 890 (1998).

[72]K. Pernal, R. Podeszwa, K. Patkowski, and K. Szalewicz, Phys. Rev. Lett. **103**, 263201 (2009).

[73]A. Edelman, T. A. Arias, and S. T. Smith, SIAM J. Matrix Anal. Appl. **20**, 303 (1998), arXiv:9806030 [physics].

[74]J. Nocedal and S. J. Wright, *Numerical Optimization*, edited by P. Glynn and S. M. Robinson, Springer Series in Operations Research and Financial Engineering (Springer-Verlag, New York, 1999) pp. 224–227.

[75]T. Van Voorhis and M. Head-Gordon, Mol. Phys. **100**, 1713 (2002).

[76]J. J. Moré and D. J. Thuente, ACM Trans. Math. Software **20**, 286 (1994).

[77]Y. Shao, L. F. Molnar, Y. Jung, J. Kussmann, C. Ochsenfeld, S. T. Brown, A. T. B. Gilbert, L. V. Slipchenko, S. V. Levchenko, D. P. O'Neill, R. A. DiStasio, R. C. Lochan, T. Wang, G. J. O. Beran, N. A. Besley, J. M. Herbert, C. Y. Lin, T. Van Voorhis, S. H. Chien, A. Sodt, R. P. Steele, V. A. Rassolov, P. E. Maslen, P. P. Korambath, R. D. Adamson, B. Austin, J. Baker, E. F. C. Byrd, H. Dachsel, R. J. Doerksen, A. Dreuw, B. D. Dunietz, A. D. Dutoi, T. R. Furlani, S. R. Gwaltney, A. Heyden, S. Hirata, C.-P. Hsu, G. Kedziora, R. Z. Khalliulin, P. Klunzinger, A. M. Lee, M. S. Lee, W. Liang, I. Lotan, N. Nair, B. Peters, E. I. Proynov, P. A. Pieniazek, Y. M. Rhee, J. Ritchie, E. Rosta, C. D. Sherrill, A. C.

Simmonett, J. E. Subotnik, H. L. Woodcock, W. Zhang, A. T. Bell, A. K. Chakraborty, D. M. Chipman, F. J. Keil, A. Warshel, W. J. Hehre, H. F. Schaefer, J. Kong, A. I. Krylov, P. M. W. Gill, and M. Head-Gordon, Phys. Chem. Chem. Phys. **8**, 3172 (2006).

[78]Y. Shao, Z. Gan, E. Epifanovsky, A. T. Gilbert, M. Wormit, J. Kussmann, A. W. Lange, A. Behn, J. Deng, X. Feng, D. Ghosh, M. Goldey, P. R. Horn, L. D. Jacobson, I. Kaliman, R. Z. Khaliullin, T. Kuś, A. Landau, J. Liu, E. I. Proynov, Y. M. Rhee, R. M. Richard, M. a. Rohrdanz, R. P. Steele, E. J. Sundstrom, H. L. Woodcock, P. M. Zimmerman, D. Zuev, B. Albrecht, E. Alguire, B. Austin, G. J. O. Beran, Y. a. Bernard, E. Berquist, K. Brandhorst, K. B. Bravaya, S. T. Brown, D. Casanova, C.-M. Chang, Y. Chen, S. H. Chien, K. D. Closser, D. L. Crittenden, M. Diedenhofen, R. a. DiStasio, H. Do, A. D. Dutoi, R. G. Edgar, S. Fatehi, L. Fusti-Molnar, A. Ghysels, A. Golubeva-Zadorozhnaya, J. Gomes, M. W. Hanson-Heine, P. H. Harbach, A. W. Hauser, E. G. Hohenstein, Z. C. Holden, T.-C. Jagau, H. Ji, B. Kaduk, K. Khistyaev, J. Kim, J. Kim, R. a. King, P. Klunzinger, D. Kosenkov, T. Kowalczyk, C. M. Krauter, K. U. Lao, A. Laurent, K. V. Lawler, S. V. Levchenko, C. Y. Lin, F. Liu, E. Livshits, R. C. Lochan, A. Luenser, P. Manohar, S. F. Manzer, S.-P. Mao, N. Mardirossian, A. V. Marenich, S. a. Maurer, N. J. Mayhall, E. Neuscamman, C. M. Oana, R. Olivares-Amaya, D. P. ONeill, J. a. Parkhill, T. M. Perrine, R. Peverati, A. Prociuk, D. R. Rehn, E. Rosta, N. J. Russ, S. M. Sharada, S. Sharma, D. W. Small, A. Sodt, T. Stein, D. Stück, Y.-C. Su, A. J. Thom, T. Tsuchimochi, V. Vanovschi, L. Vogt, O. Vydrov, T. Wang, M. a. Watson, J. Wenzel, A. White, C. F. Williams, J. Yang, S. Yeganeh, S. R. Yost, Z.-Q. You, I. Y. Zhang, X. Zhang, Y. Zhao, B. R. Brooks, G. K. Chan, D. M. Chipman, C. J. Cramer, W. a. Goddard, M. S. Gordon, W. J. Hehre, A. Klamt, H. F. Schaefer, M. W. Schmidt, C. D. Sherrill, D. G. Truhlar, A. Warshel, X. Xu, A. Aspuru-Guzik, R. Baer, A. T. Bell, N. a. Besley, J.-D. Chai, A. Dreuw, B. D. Dunietz, T. R. Furlani, S. R. Gwaltney, C.-P. Hsu, Y. Jung, J. Kong, D. S. Lambrecht, W. Liang, C. Ochsenfeld, V. a. Rassolov, L. V. Slipchenko, J. E. Subotnik, T. Van Voorhis, J. M. Herbert, A. I. Krylov, P. M. Gill, and M. Head-Gordon, Mol. Phys. **113**, 184 (2015).

[79]K. U. Lao and J. M. Herbert, J. Phys. Chem. A **119**, 235 (2015).

[80]J. Witte, M. Goldey, J. B. Neaton, and M. Head-Gordon, J. Chem. Theor. Comput. **11**, 1481 (2015).

[81]T. H. J. Dunning, J. Chem. Phys. **90**, 1007 (1989).

[82]R. A. Kendall, T. H. J. Dunning, and R. J. Harrison, J. Chem. Phys. **96**, 6796 (1992).

[83]D. Rappoport and F. Furche, J. Chem. Phys. **133**, 134105 (2010).

[84]See supplemental material at URL for data and discussion on the basis set convergence of newly introduced terms.

[85]C. Edmiston and K. Ruedenberg, Rev. Mod. Phys. **35**, 457 (1963).

[86]See supplemental material at URL for plots demonstrating correct asymptotic behavior.

[87]S. Tsuzuki, K. Honda, T. Uchimaru, and M. Mikami, J. Chem. Phys. **120**, 647 (2004).

[88]T. Janowski and P. Pulay, J. Am. Chem. Soc. **134**, 17520 (2012).

[89]P. M. Gill, B. G. Johnson, and J. a. Pople, Chem. Phys. Lett. **209**, 506 (1993).

[90]S. Grimme, Ang. Chem. Int. Ed. **47**, 3430 (2008).